Instabilities in the flow of thin films on heterogeneous surfaces

Lou Kondic[(1)] **and Javier A. Diez**[(2)]

[(1)] Department of Mathematical Sciences and
Center for Applied Mathematics and Statistics
New Jersey Institute of Technology, Newark, NJ 07102

[(2)] Instituto de Fisica Arroyo Seco
Universidad Nacional del Centro
de la Provincia de Buenos Aires

Pinto 399 - 7000 - Tandil, Argentina

CAMS Report 0304-03, Fall 2003

Center for Applied Mathematics and Statistics

NJIT

Instabilities in the flow of thin films on heterogeneous surfaces

Lou Kondic*

Department of Mathematical Sciences & Center for Applied Mathematics & Statistics

New Jersey Institute of Technology, Newark, NJ 07102

Javier Diez†

Instituto de Física Arroyo Seco, Universidad

Nacional del Centro de la Provincia de Buenos Aires

Pinto 399, 7000, Tandil, Argentina

(Dated: August 31, 2003)

Abstract

We present computational and experimental results about instability development in the gravity driven flow of thin fluid films on heterogeneous surfaces. In particular, we concentrate on the dynamics of the fluid fronts, i.e., on the contact line. We show that heterogeneity of the solid surface can have significant effect on the flow dynamics. Since the effect of heterogeneity often competes with the basic instability mechanism that would occur even on homogeneous surfaces, the result is an elaborate interplay of various instability mechanisms. The computational results presented here outline both the flow on surfaces perturbed by regular patterns, and on surfaces perturbed by irregular, noise-like perturbations. We relate these computational results to the pattern formation process in our experiments of gravity driven flow down an incline. Good qualitative agreement is found between the simulations and the experiments.

The flow of thin films is relevant in a number of different fields, such as engineering, biology, and chemistry. These flows can be driven by gravity, or various other forces of mechanical, thermal or electromagnetic origins. In many situations, the fluid fronts become unstable, leading to formation of finger-like or triangular saw-tooth patterns, and resulting in uneven or partial surface coverage. Very often, these instabilities are undesirable in technological applications since they may lead to formation of dry regions or other defects. In other applications, however, partial wetting is actually preferred since surfaces that are selectively wetted on microscale can be used as the base for various MEMS devices.

In this work, we concentrate on perhaps the simplest of thin film flows - gravity driven flow down an inclined plane. Experiments are usually performed by releasing fluid in some controllable fashion at the top of an incline. After some time, the initially straight contact line, where liquid, gas, and solid phase meet, becomes unstable with respect to transverse perturbations. It has been conjectured that this instability is related to the formation of a capillary ridge in the fluid profile, just behind the advancing contact line. Silvi and Dussan[1] expanding on the pioneer work by Huppert[2] show that the fluid wetting properties play an important role in instability development and the degree of surface coverage. Recently, the experiments by Johnson[3] and Johnson et al.[4], as well as computations by Diez and Kondic[5] and Kondic and Diez[6] show that another important parameter is the inclination angle. Decrease of inclination angle not only reduces the patterns growth rate, but it also modifies their shape: while large angles lead to fingers characterized by almost straight sides, smaller angles lead to formation of triangular saw-tooth patterns.

Theoretically, the fluid film's dynamics is typically approached using lubrication approximation. Within this framework, an initial insight into the instability results from linear stability analysis (LSA). Troian et al.[7] perform LSA for the flow down a vertical plane and show that there is a band of unstable modes, with short wavelengths stabilized by surface tension. Spaid and Homsy[8] and Bertozzi and Brenner[9] extend this analysis to the general case of flow down an inclined plane, and show that the normal component of gravity (hydrostatic term) shifts the mode of maximum growth to longer wavelengths, and also tends to stabilize the flow by decreasing the instability's growth rate. This stabilizing effect appears to be so strong that it is predicted to completely remove the instability for very small inclination angles, in contradiction to experiments. In Ref. 9, a transient growth approach is used to explain this discrepancy, while Ye and Chang[10] use spectral theory to reach the

same goal. Both works analyze propagation and amplification of noise from the substrate to the fluid front, although they employ different methods. Grigoriev[11] analyzes the transient growth and related effects in the flow of thermally driven films. Very recent paper by Davis and Troian[12] claims that the influence of transient growth mechanism is weaker than previously thought for gravity driven thin films.

The flow on heterogeneous surfaces has also been recently considered by a number of authors. Kalliadasis, Bielarz, and Homsy[13], and Bielarz and Kalliadasis[14] discuss (quasi) 2D and 3D flow, respectively, over trenches which are of comparable lengthscale to the film height, similarly to the earlier work by Stillwagon and Larson[15]. A concept of nonuniform slip coefficient has been applied to thin film flows by Hoffman *et al.*[16] and Wang[17], building upon previous works by Hocking[18] and Miksis and Davis[19]. Modifications of contact angle in the spreading of drops on chemically heterogeneous substrates were analyzed experimentally by Drelich *et al.*[20], and computationally by Schwartz[21] and Schwartz and Elley[22]. Series of papers by Troian and coworkers[23–26] considers selective, controlled wetting of a chemically heterogeneous substrate. Garnier et al.[27] propose use of thermal feedback control to suppress the contact line instability. Dewetting of heterogeneous substrates has been also analyzed recently, e.g., by Brusch *et al.*[28], and Kargupta and Sharma[29]. We will see later that some results presented in our work have common features to the results presented in Refs. 28,29, although the systems considered are rather different.

Our previous works[5,6] analyzed instability development in the flow of thin films on homogeneous surfaces, while in Kondic and Diez[30] we briefly outlined the influence of controlled surface perturbations ('channels' of varying flow resistance). In this work, we concentrate more generally on the influence of surface heterogeneity on the instability development. This study is partially motivated by an earlier work by Kondic and Bertozzi[31] which has shown that substrate perturbations can play a role in the development of instability. However, that work reached this conclusion indirectly, by recording the influence that a substrate perturbation has on the capillary ridge's height, which is itself related to instability development. Here, we report results of fully nonlinear simulations in (quasi) $3D$ system within the framework of lubrication approximation. We note that in this work we assume complete wetting, and do not discuss in any detail issues related to non-zero contact angle. An interested reader can find significant material regarding partial wetting in recent works that discuss disjoining-pressure model (e.g., Bertozzi *et al.*[32], Glasner and Witelski[33]) or related diffuse

interface model (e.g. Pismen and Pomeau[34], Thiele *et al.*[35]).

The main goals of this paper are twofold. First, we show how various imposed surface perturbations, localized or not, lead to formation of regular patterns. Next, we analyze how these regular patterns are modified by the presence of surface noise. Some of the results are illustrated by experiments involving the flow of very viscous Newtonian fluid down an inclined plane in both (macroscopically) homogeneous and on patterned surfaces.

I. FORMULATION OF THE PROBLEM

Dynamics of thin liquid films is typically analyzed within the framework of lubrication approximation. The assumptions of this approach, as well as the details of our computational methods are given elsewhere; see Diez and Kondic[36] and the references therein. For completeness, here we give a basic outline, concentrating mostly on the aspects relevant to the main subject of this work.

Within the lubrication approximation, one uses the fact that the film thickness is much smaller than any in-plane dimension. After depth-averaging the fluid velocity over this short direction, and using no-slip boundary condition at the solid-liquid interface, the continuity equation yields the following equation for the height, h, of the (incompressible) liquid film:

$$\frac{\partial h}{\partial t} = -\frac{1}{3\mu}\nabla \cdot \left[\gamma h^3 \nabla\nabla^2 h - \rho g h^3 \nabla h \cos\alpha + \rho g h^3 \sin\alpha \ \mathbf{i}\right], \tag{1}$$

where $\nabla = (\partial_x, \partial_y)$, x points down the incline, and y in the transverse direction. Here, $\mu, \rho, g, \gamma, \alpha$ are the viscosity, density, gravity, surface tension, and the inclination angle, respectively. The fourth order term results from surface tension, and the last two terms are due to gravity.

To balance viscous and capillary forces in Eq. (1), we scale h by the fluid thickness far behind the contact line, h_c, and define the scaled in-plane coordinates and time by $(\bar{x}, \bar{y}, \bar{t}) = (x/x_c, y/x_c, t/t_c)$, where

$$x_c = \left(\frac{a^2 h_c}{\sin\alpha}\right)^{1/3}, \qquad t_c = \frac{3\mu}{\gamma}\frac{a^2 x_c}{h_c^2 \sin\alpha}, \tag{2}$$

and $a = \sqrt{\gamma/\rho g}$ is the capillary length. The velocity scale is chosen naturally as $U = x_c/t_c$, and the capillary number is defined as $Ca = \mu U/\gamma$. Using this nondimensionalization,

Eq. (1) for $\bar{h} = h/h_c$ is given by (dropping the bars)

$$\frac{\partial h}{\partial t} + \nabla \cdot \left[h^3 \nabla \nabla^2 h\right] - D(\alpha) \nabla \cdot \left[h^3 \nabla h\right] + \frac{\partial h^3}{\partial x} = 0 \ , \tag{3}$$

where the single dimensionless parameter $D(\alpha) = (3Ca)^{1/3} \cot(\alpha)$ measures the size of the normal component of gravity.

All theoretical and computational methods require some regularizing mechanism - either assuming a small foot of fluid in front of the apparent contact line (precursor film, see[7–9]), or relaxing the no-slip boundary condition at fluid-solid interface (see e.g., Greenspan[37], Dussan[38], or Hocking and Rivers[39]). Diez, Kondic, and Bertozzi[40] have recently performed an extensive analysis of the computational performance of these regularizing mechanisms applied to the spreading drop problem. In that paper it is shown that the results are rather insensitive to the choice of model, consistently with, e.g., Ref. 8. However, the computational performance of the precursor film model is shown to be much better than that of various slip models.[40] For this reason, here we also use a precursor film of thickness b (scaled by h_c) as a regularizing method.

The computational domain is chosen as a rectangle defined by $0 \leq x \leq L_x$ and $0 \leq y \leq L_y$ which is divided into $N_x \times N_y$ cells centered at node points (x_i, y_j) with $i = 1, ..., N_x$ and $j = 1, ..., N_y$. Equation (3) is then discretized in space using a central finite difference scheme. The boundary conditions are chosen to model constant fluid flux far behind the fluid front. That is, we assume that there is an infinite stream of fluid far behind the front, that keeps the fluid height constant there. Within our nondimensionalization scheme, this leads to $h(0, y, t) = 1$. We require that far ahead of the moving front, the fluid height is equal to the precursor thickness, $h(L_x, y, t) = b$, and also that the streamwise gradients of the fluid height vanish at the boundaries, i.e., $h_x(0, y, t) = h_x(L_x, y, t) = 0$. At the boundaries $y = 0$ and $y = L_y$, it is convenient to use $h_y(x, 0, t) = h_y(x, L_y, t) = 0$, $h_{yyy}(x, 0, t) = h_{yyy}(x, L_y, t) = 0$. This choice enforces no-flow across these boundaries. Since the tangential component of the fluid flux is let free, these boundaries could be thought of as 'slipping walls'.

Time discretization is performed using implicit Crank-Nicolson scheme. The advantages of an implicit scheme for this problem are obvious: the stability requirement for an explicit scheme is that $\Delta t < C min[\Delta x, \Delta y]^4$, where Δt is a time step, and C is a positive constant. Thus, an explicit scheme requires very short time steps for a reasonable spatial accuracy. In our simulations, time steps are chosen dynamically based on prescribed accuracy, and the

obvious requirement that the computed solution is strictly positive.[36]

The nonlinear system of algebraic equations that results after time discretization is linearized using Newton method; the linearized problems are then solved using iterative biconjugate gradient method. As a typical grid spacing we use $dx = 0.2,\ dy = 0.25$, leading to about $200 - 400$ grid points in each direction. More details regarding efficiency, computational cost, and other issues such as convergence and accuracy are given in Ref. 36.

II. MAIN FEATURES OF THE FLOW ON A HOMOGENEOUS SURFACE

Linear stability analysis[7–9] of the governing Eq. (3) has shown that the flow is unstable with respect to fluid front perturbations in the transverse direction. LSA is performed by expanding to the first order all nonlinear terms in Eq. (3) about the base state. This base state is obtained as the y independent solution of Eq. (3) in a reference frame moving with velocity $u = 1+b+b^2$[7]. It is characterized by the presence of a capillary ridge, which appears to be closely related to the onset of instability.[7–9]

The main results of LSA is that long wavelengths are unstable, while the short ones are stabilized by surface tension, represented by the fourth order term in Eq. (3). Consequently, there is a band of unstable modes bounded by the wavenumbers $q = 0$ and $q_c = 2\pi/\lambda_c$, where $\lambda_c \approx 8$ for $D = 0$[7]. The wavelength of maximum growth is approximately $\lambda^* \approx 12 - 14$. Although LSA is valid for short times only, one expects that the distance between resulting patterns in actual experiments is close to this wavelength.

For future reference, we note here the influence of some of the parameters on the LSA results. Increase/decrease of the precursor film thickness leads to a decrease/increase of the growth rate of the emerging patterns. This observation was used in recent work[30] which showed that perturbing precursor thickness in a controllable manner could induce instability and occurrence of regular patterns. The influence of (noise-induced) precursor thickness perturbations on the flow stability for very small inclination angles was also analyzed in some detail in a number of recent works.[9,10,12,30]

Figure 1 shows an example of our recent computational results for the flow down a homogeneous vertical ($D = 0$) substrate.[5,6] These results confirm the main predictions of LSA. Here, the initial condition is formulated by perturbing the base state (an example of a base state in 2D can be seen in Fig. 4b) by a superposition of $N = 100$ modes characterized

by wavelengths $\lambda_{0,i} = 2L_y/i$, $i = 1, ..., 100$. Each mode is assigned a random amplitude in the range $[-0.1, 0.1]$. This initial profile is shown in Fig. 1a. In Fig. 1b we see formation of long finger-like patterns that result for later times. These fingers are characterized by nonuniform lengths, resulting from irregular initial conditions. This nonuniformity is also related to the fact that the distance between the fingers varies, although it is on average close to λ^* from LSA. Additional simulations which use different distributions of initial wavelengths and different domain size show that this average value is close to 12. More details regarding the influence of the inclination angle (controlled by the parameter D) on the pattern formation is available elsewhere.[5,6] Here we provide a brief illustration by presenting results from physical experiments.

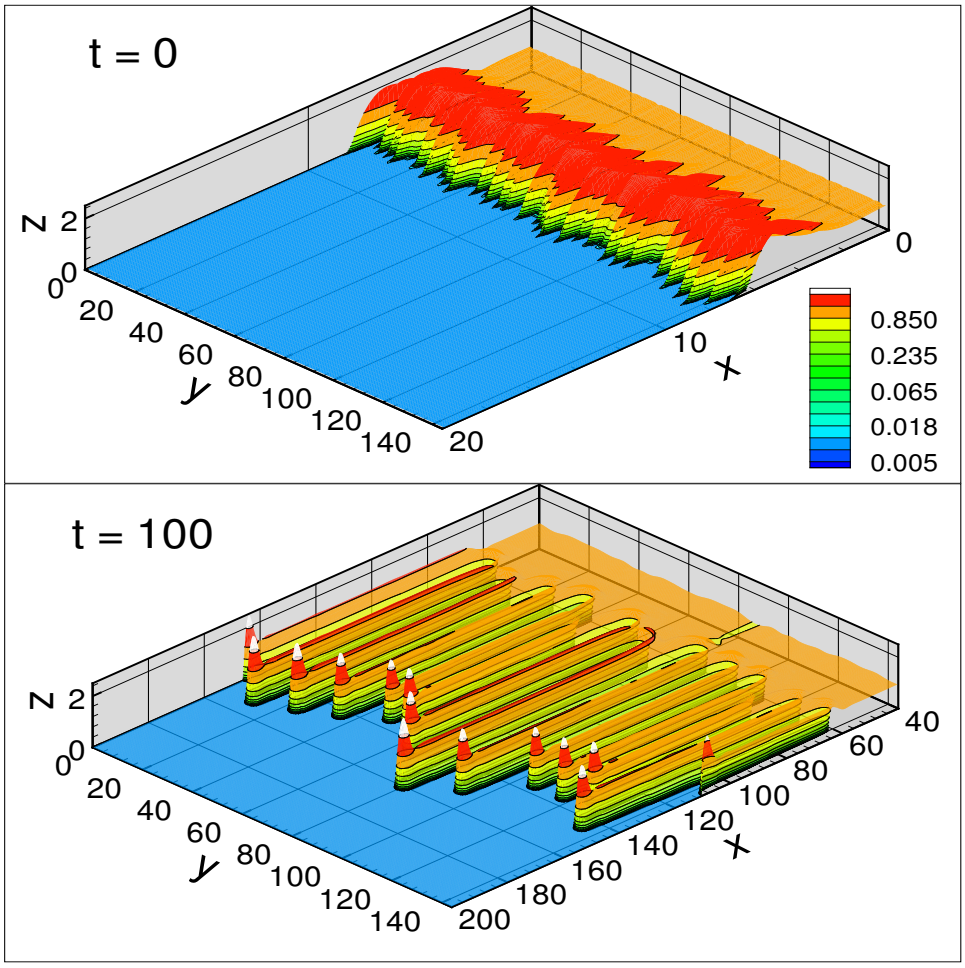

FIG. 1: Contour plot of the fluid thickness. Initial profile is perturbed by a superposition of 100 modes characterized by random amplitudes. Here $D = 0$ and $b = 0.01$. Note that the z scale is considerably stretched for presentation purposes ($L_y = 144$).

The experiments are performed on a glass surface of dimensions of 100 by 50 cm, using fixed amount (typically, 25 g) of wetting fluid (polydimethylsiloxane (PDMS), AlfaAesar Ward Hill, MA), also known as silicon oil (viscosity: 50 cSt; surface tension: 21 dyn/cm, density 0.96 g/cm^3). The fluid is released close to the top of the plane using a simple mechanical "dam" consisting of a piece of rubber fixed to a metal frame. The surface is prepared by cleaning it with soap and water. No efforts are made to remove PDMS from the previous runs from the glass surface, which can therefore be thought of as prewetted by the fluid. More details about experimental techniques as well as a pedagogical explanation of details of the instability development are available in the paper by Kondic[41].

Figure 2 shows the developed patterns for three inclination angles: $\alpha = 90°$ (a), $\alpha = 30°$ (b), and $\alpha = 5°$ (c). These experimental results clearly show how the inclination angle influences the instability development: for smaller α (larger D), the instability develops slower, the wavelengths increase, and the evolving pattern shape changes smoothly from finger-like to triangular. These main features are in qualitative agreement with the computational results presented in Fig. 1 for $D = 0$ and in Refs. 5,6 for $D > 0$. For a more precise agreement, the simulations need to be adjusted for the fact that the experiments are performed using finite amount of fluid. We analyze the issues related to fluid thinning elsewhere,[44] and concentrate here on the (constant flux) flow on inhomogeneous surfaces.

Before proceeding, we note that LSA, as well as the computations such as those yielding the results presented in Fig. 1 assume presence of small perturbations of the contact line in the transverse direction. These perturbations are necessarily present in any physical experiment. However, for simplicity of presentation, and since in this work we are predominantly interested in the inhomogeneities of surface itself, we mostly ignore these perturbations, and refer to them only briefly in connection to the experimental results presented in Sec. VI. Most of the computational results are obtained assuming $D = 0$ (i.e., flow down a vertical plane), with the influence of nonzero D briefly outlined where appropriate so to relate the computations to experiments.

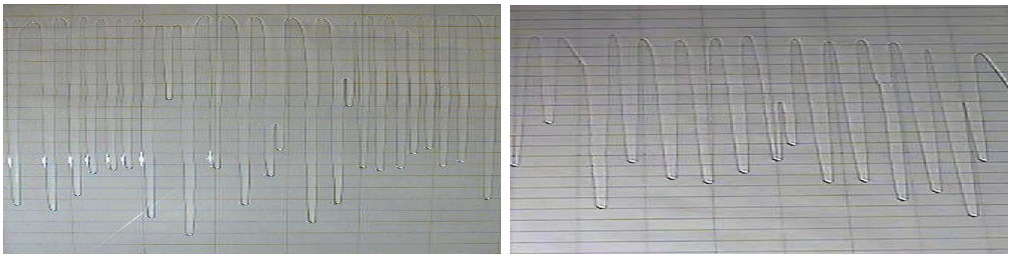

(a) $\alpha = 90°$, time = 33 sec.

(b) $\alpha = 30°$, time = 38 sec.

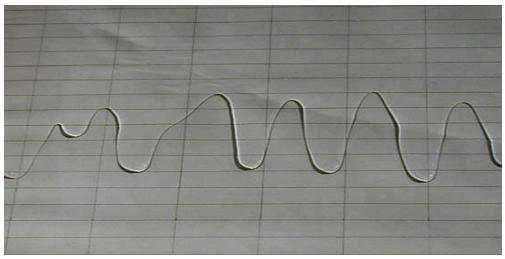

(c) $\alpha = 5°$, time = 120 sec.

FIG. 2: Development of instability in physical experiments. Here, 25 g of PDMS is released at the top of a glass surface characterized by the inclination angle α. The rectangles' width (in the streamwise direction) is 2 cm, and their length is 5 cm.

III. BASIC INSTABILITY MECHANISM OF THE FLOW ON INHOMOGENEOUS SURFACES

We model substrate inhomogeneity by perturbing the precursor film thickness. While it might appear that imposing perturbations of this kind is rather restrictive since a precursor film is not always present in physical experiments or technological applications, this approach is actually quite general. A number of works, including de Gennes[42] have shown that the main flow features are not influenced significantly by the choice of regularizing method at the contact line. One could allow for the presence of a precursor film, include possibility of fluid slip, or assume that van der Waals forces at the liquid-solid interface are important; for the macroscopic flow properties (in particular, instability development), the main factor is the actual length-scale that is introduced at the front. Since this length-scale determines the degree of energy dissipation, one expects that its spatial variation can have significant

influence on the macroscopic flow properties, as shown in the case of spatially dependent slip coefficient.[16,18]

Recent work[31] analyzed the influence that a localized perturbation of the precursor thickness had on the flow in (quasi) 2D geometry (the y direction is ignored). Figure 3 shows an example of these results: as the fluid's main body flows over a perturbation (imposed at $x = 20$ in Figure 3), the capillary ridge's height is increased, implying, as pointed out above, that the flow stability properties may be modified. Correspondingly, it is reasonable to assume that surface inhomogeneities might lead to flow instabilities. Figure 3a shows an amplified perturbation: a precursor's modification on the scale of 1% of the thickness of the fluid's main body leads to a large increase of the capillary ridge's height. However, this happens only if the perturbation is sufficiently wide. This is illustrated by Fig. 3b, where the perturbation is of the same depth, but it is much more narrow. Here, the fluid practically does not 'see' the perturbation. This result is consistent with the solutions describing planarization during spin coating over perturbations (trenches) whose depth is comparable to the thickness of the fluid's main body.[15]

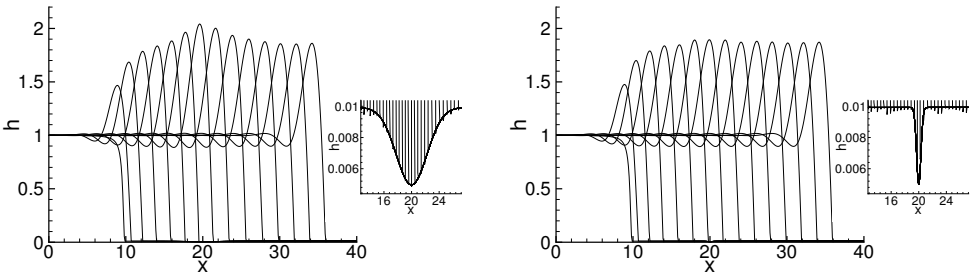

(a) Wide perturbation.

(b) Narrow perturbation.

FIG. 3: Snapshot of the 2D fluid profile as it flows over a precursor perturbation. The insets show the zoomed-in perturbation region around $x = 20$. The unperturbed precursor thickness is $b = 0.01$, barely visible on the scale of the fluid's main body.

As mentioned above, 2D simulations deduced the influence of surface perturbations on the instability indirectly, through changing the capillary ridge's height. However, 3D simulations are needed to understand this effect in detail. In particular, 2D simulations show that relatively large extend of a perturbation in the streamwise direction is needed to significantly

influence the capillary ridge's height; it is not obvious a priori that this result can be carried over to 3D geometry.

Therefore, we now proceed to 3D geometry, and analyze the main effect that localized perturbations (dips) of the precursor have on the flow stability. These perturbations are 3D extensions of the 2D perturbations used in Fig. 3. They have a flat central region of a given depth, δ (in units of b), and a transition region surrounding the flat part that provides a smooth change from the perturbations' bottoms to the unperturbed precursor (see Fig. 4a for an example). These transition regions are needed since lubrication approximation assumes weak gradients of the fluid thickness, with which a sharp interface between the perturbations and the unperturbed precursor would not be consistent. On the perturbations' sides, the thickness of these transition regions is specified as $b(s) = b[1 - \delta \exp(-\Delta_s(s - s_c)^2)]$, where $s = [x,\ y]$, $\Delta_s = [\Delta_x,\ \Delta_y]$ defines the width of this transition region, and s_c is the position of a given perturbation's bottom edge. We note that the results are almost insensitive to the particular functional form assigned to $b(s)$, or to the value given to Δ_s. We use $\Delta_s = 4$, which gives a reasonable (O(1)) width. In the presentation that follows, we report total effective perturbation widths, w_x, w_y, as the widths (in the x, y directions) of the regions where the precursor thickness is less than $b(1 + \delta)/2$.

Figure 4 shows an example of our results for the flow down a vertical plane ($D = 0$), and for unperturbed $b = 0.01$. At $t = 0$, the time evolution is started from initial condition obtained from 2D simulations. There are no contact line's perturbations imposed at $t = 0$, in contrast to Fig. 1. The precursor perturbations are centered at $x = 12$, $y = 8,\ 24$, and their effective widths are $w_x = w_y = 3$.

In Fig. 4, we see that the fluid's main body flows uniformly under gravity until it reaches the perturbations. There, the flow is slowed down. This slowdown can be understood by recalling that smaller b provides more resistance to the flow in the perturbed regions (note that $b \to 0$ limit is singular; for $b = 0$, the no-slip boundary condition would not permit any contact line's dynamics). Instead, the fluid escapes to the "easy" flow regions in between the 'obstacles'. Larger amount of fluid in these easy regions leads to an increase of fluid velocity there (velocity is approximately proportional to h^2, see e.g. Ref. 6), and hence to the instability. As a result, finger-like patterns form. These are similar to those shown in Fig. 1, where the contact line itself was perturbed (in Fig. 4, the domain is much more narrow so there is room for only two fingers). In Fig. 4c, we see that the fluid in the easy

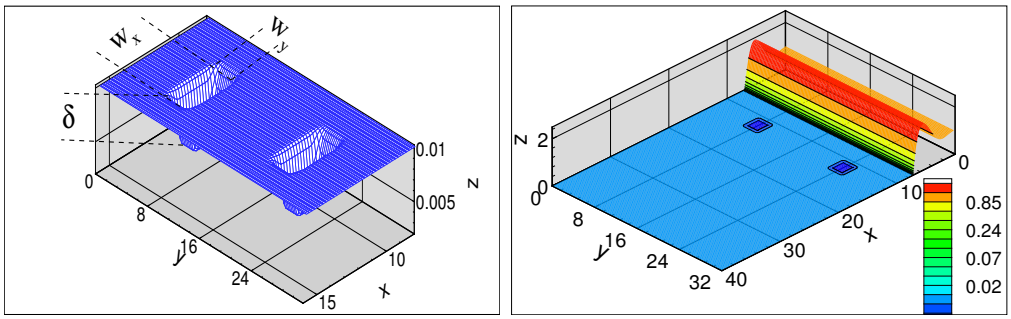

(a) Zoom-in view of the perturbed area of the otherwise featureless precursor film.

(b) $t = 0$.

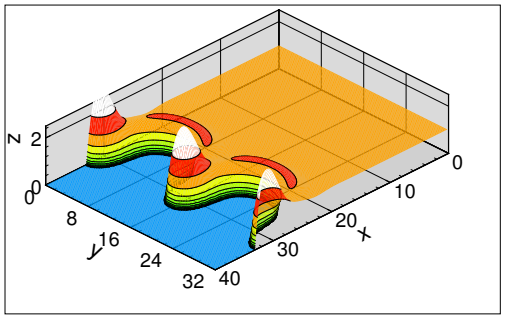

(c) $t = 20$.

FIG. 4: Contour plot of the fluid thickness. The initially flat fluid front shown in (b) flows over perturbed precursor and develops an unstable front shown in the part (c). Part (a) shows zoom-in view of perturbations characterized by the depth $\delta = 0.5$ (in the units of b), and by effective widths $w_x = w_y = 3$, as explained in the text. Here $D = 0$, $b = 0.01$; note that $y = 16$ is the symmetry line.

flow regions is characterized by an increased height of its capillary ridge, while much smaller capillary ridge is present in the roots regions, flowing over the perturbations. This fluid profile, while expected (given its similarity to the profile shown in Fig. 1), is not necessarily obvious from the 2D results, where the capillary ridge is higher as the fluid passes over perturbations. There is a major difference between 2D and 3D results: in the 2D case, the fluid does not have a possibility of forming structures in the transverse direction in order to find an energetically more favorable state.

IV. PARAMETRIC DEPENDENCE

There are a number of factors that influence the instability development. First, we have factors related to the basic flow configuration: inclination angle, precursor film thickness, and domain size in the transverse direction. These factors have been analyzed in some detail elsewhere.[5,6] Next, we have parameters introduced by the perturbations: their size, shape, depth, and distribution. We outline the influence of each of these parameters separately, with obvious restrictions introduced by exploring only slices of the available phase space. In particular, we note that the domain size in the transverse direction has a significant influence on the emerging patterns distribution, due to the boundary conditions enforced there. In order to at least partially eliminate the influence of this parameter, some of the simulations presented here are performed in large domains, so that the fluid has significant freedom in choosing its shape, without being influenced by the boundaries. On the other hand, some results can be easier understood in smaller domains, where emerging patterns are typically simpler. The influence of selected parameters is presented in the figures of this section; the rest is illustrated in Table I, to which we refer throughout. If not specified differently, we use $D = 0$, $b = 0.01$, $w_x = w_y = 3$, and $\delta = 0.5$.

Distance between perturbations. Figure 5 shows how instability is being modified as the distance between perturbations is decreased from $d = 24$ (a) to 4 (d). The perturbations are otherwise identical to the ones used in Fig. 4.

First, we realize that the distance between emerging patterns is influenced not only by the spacing d between perturbations, but also by the boundary conditions, which require formation of either a tip or a root there. The interplay between these two factors leads to various λ's, which may or may not be equal to d. However, these emerging λ's do center around λ^*. In the examples shown in Fig. 5, the 'primary' wavelengths (that develop first) vary between $\lambda = 32/3$ (a) and $\lambda = 16$ (b, c, d). In some cases, additional (secondary) instability develops, such as $\lambda = 8$ in Fig. 5d. If the distance between the surface perturbations falls below $\lambda_c \approx 8$, there is no pattern formation in between (viz. Fig. 5d). These perturbations do, however, induce instability in the rest of the domain.

Still basing our argument on LSA, we can also estimate the growth rates of various patterns. Since, to the leading order, the growth rate is determined by λ, one can predict that the emerging patterns shown in Fig. 5a should grow slower than the ones shown in

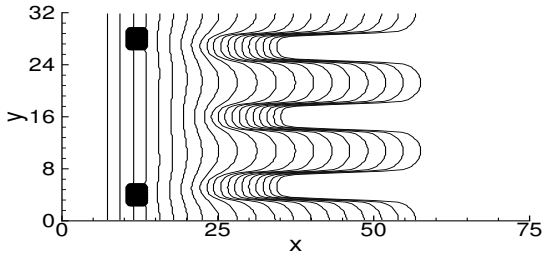

(a) *Distance between perturbations:* $d = 24$.

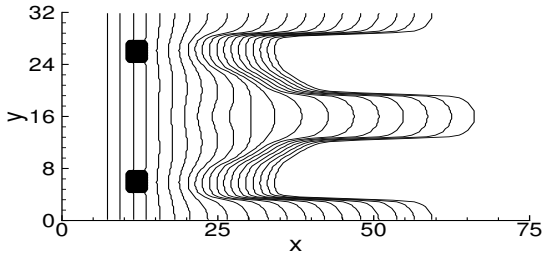

(b) $d = 20$.

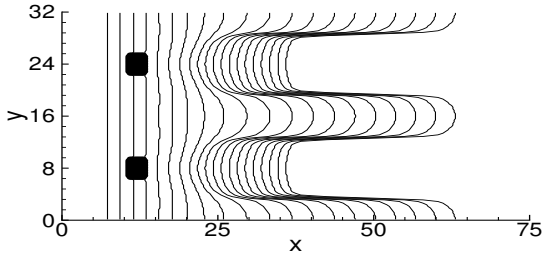

(c) $d = 16$.

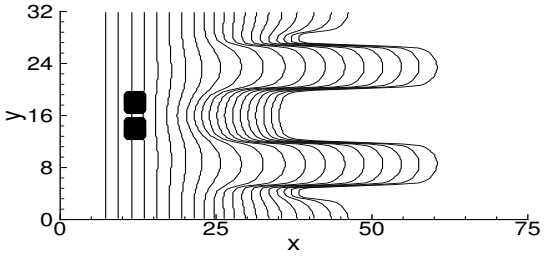

(d) $d = 4$.

FIG. 5: Snapshots of the fluid front as it flows over the perturbations shown by dark areas. The distance between the perturbations, d, is varied as shown in the figures. The fluid front's positions are plotted in $\delta t = 2$ intervals.

Fig. 5c. Also, the patterns shown in Fig. 5b, c grow faster than the ones in Fig. 5d, since the latter is slowed down by the secondary $\lambda = 8$ instability.

It is also interesting to notice the competition between different λ's in Fig. 5b. Here, $d = 20$ excites initial formation of two patterns in between the perturbations. These patterns merge into one eventually. However, this merge does not happen in Fig. 5a, where $d = 24$. Therefore, Figs. 5a - b show that the minimum distance for formation of multiple patterns is between 20 and 24, which is comparable to $2\lambda_c$. These results are consistent with the simulations of dewetting process on chemically heterogeneous substrates, where formation of stable patterns is observed when the imposed perturbation is characterized by a lengthscale between λ_c and $2\lambda_c$.[29] Additional simulations (and experiments such as those presented in Sec. VI C) have shown that the exact 'critical' distance is influenced by a number of factors, including noise in experiments, and the computational domain's size (see also Ref. 30).

Perturbation width and depth. Based on the 2D results[31], we expect rather strong influence of the perturbation width and depth on the instability. Table Ia - c shows that this is really the case, at least for the small domain size considered here. Essentially, increasing the perturbed regions' width (both in the x and y directions) and the depth speeds up the development of instability. This effect saturates for large widths and depths. In particular for late times (an example is $t = 60$ in Table Ia - c), there is not much difference in the emerging patterns length for sufficiently large perturbations.

Inclination angle. It is known that changing the inclination angle has a profound influence on the development of instability.[3,5,6] The pattern's growth is reduced, their shape is changed from finger-like to triangular saw-tooth shape, and the distance between patterns is increased. These results were obtained in experiments[3] (see also Fig. 2), and in our computations where instability is initiated by perturbing the contact line. Here we explore computationally the inclination angle's influence when the instability is produced by perturbing the precursor.

Figure 6 shows snapshots of the developed patterns for $D = 0,\ 1,\ 2$ and $w_x = w_y = 3$. Obviously, an increase in D leads to a drastic effect; in particular, for $D = 2$, the instability is all but completely removed. Figure 6 shows the results for the flow over perturbations characterized by relatively large extend in both x and y directions; of course, as the perturbations size is decreased, the instability is reduced even more (see Table Id for the case $w_x = w_y = 1$). The shape of emerging patterns is being modified compared

D	w_x	w_y	δ	n	$t = 10$	$t = 20$	$t = 60$
a)							
0	1	1	0.5	1	0.0	1.6	7.2
0	1	2	0.5	1	0.2	3.0	28.8
0	1	3	0.5	1	0.2	4.2	40.2
0	1	5	0.5	1	0.4	6.8	42.8
0	1	7	0.5	1	0.4	6.8	44.4
b)							
0	1	1	0.5	1	0.0	1.6	7.2
0	2	1	0.5	1	0.2	3.0	40.8
0	3	1	0.5	1	0.2	4.6	42.4
0	5	1	0.5	1	0.4	5.8	45.2
0	7	1	0.5	1	0.4	8.4	45.2
c)							
0	3	3	0.9	1	0.2	3.0	40.4
0	3	3	0.7	1	0.4	7.0	45.4
0	3	3	0.5	1	0.6	9.0	46.0
d)							
0	1	1	0.5	1	0.0	1.6	7.2
1	1	1	0.5	1	0.0	0.0	2.4
2	1	1	0.5	1	0.0	0.0	0.0
e)							
1	1	2	0.5	1	0.2	0.0	4.8
1	1	2	0.5	3	0.2	0.4	6.4
1	1	2	0.5	5	0.2	0.4	8.0
1	1	2	0.5	10	0.2	0.4	10.4

TABLE I: The table shows the pattern lengths at three different times as the fluid flows over a perturbation at $x = 12$, $y = 8$, for $L_y = 16$, and $b = 0.01$. We vary the inclination angle (measured by D), effective perturbation's width (w_x and w_y); the perturbation depth in units of b (δ), and the number of perturbations, n, in the x direction.

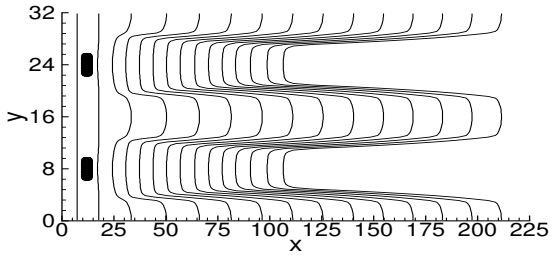

(a) $D = 0$; $0 < t < 140$.

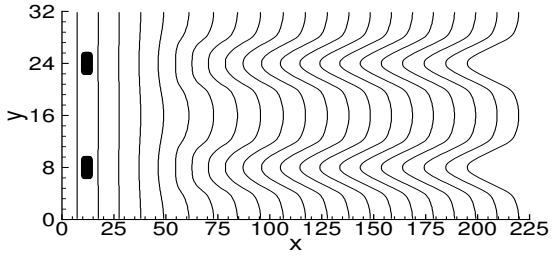

(b) $D = 1$; $0 < t < 200$.

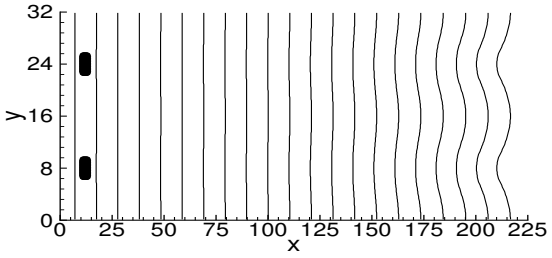

(c) $D = 2$; $0 < t < 200$.

FIG. 6: Snapshots of the fluid profile in $\delta t = 10$ intervals for different surface's inclination angles. Note increased x range and longer simulations times.

to the case of $D = 0$, in a manner similar to the case of patterns induced by contact line's perturbations.[5]

The weakening of instability as D is increased is as expected from the 2D simulations[31] and experiments.[3] However, careful inspection of Fig. 6c shows an interesting additional effect that can not be deduced from the 2D simulations. For larger D's, a precursor's perturbation leads to a localized disturbance of the front (barely visible in Fig. 6c about

time $t = 20$), which 'disappears' for extended period of time, only to start growing again about $t = 150$. This effect can be also seen for $D = 1$ in Fig. 6b, although the delay is shorter. We hope that this observation of delayed instability will provide some insight into the still open question of the cause of instability for very small inclination angles.

After outlining the basic idea of how various parameters influence the flow stability, we now proceed to explore the instability development in more complex configurations.

V. CUMULATIVE EFFECTS OF MULTIPLE PERTURBATIONS AND INSTABILITIES IN LARGE DOMAINS

The results of the preceding section concentrate on the parametric dependence of the basic instability mechanism induced by one or two perturbations in relatively narrow computational domains. In physical experiments, one expects the presence of multiple perturbations, so it is of interest to explore computationally the effect of more perturbations. Also, experiments are typically performed in wide domains, so that the boundary effects are apparent only at the edges; by performing simulations in domains that compare well with experimental ones we hope to obtain more realistic results. Note in particular that our boundary conditions at the side walls (see Sec. I) require vanishing of the solution's normal derivative, so that either root or tip must develop there. In narrow computational domains, this requirement obviously has an influence on the emerging wavelengths, i.e. on the separation between fingers. By increasing the domain's width, we remove (or at least reduce) this effect.

Cumulative effect of multiple perturbations. Figure 7 shows the effect that increasing number of perturbations that follow each other in the streamwise direction has on the flow (the emerging patterns lengths are also given in Table Ie). There is clearly an effect on the long time dynamics: more perturbations lead to an increased instability. This effect, however, is not very strong. Table Ie shows approximately two-fold increase of the emerging pattern's length between $n = 1$ and $n = 10$ at $t = 60$. For longer times, this difference even decreases. The limiting case, where all perturbations are touching each other, leading to continuous channels, has already been briefly discussed in a separate publication.[30]

Large domains and single perturbation. In the figures presented until now, the emerging wavelengths are influenced significantly by the problem's geometry. In the simulations that follow, we allow the system to have a high degree of freedom in choosing the emerging

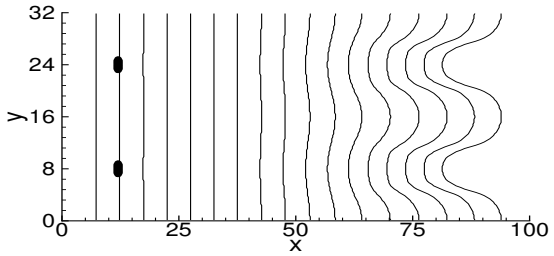

(a) $n = 1$.

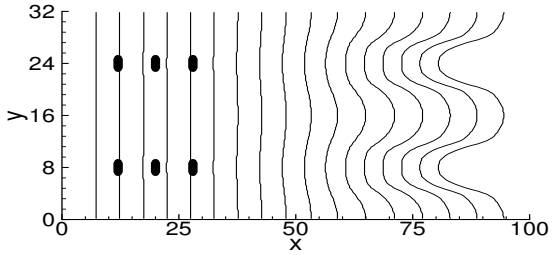

(b) $n = 3$.

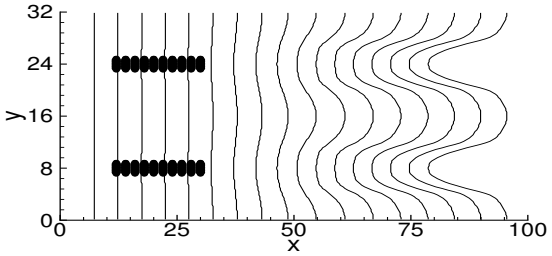

(c) $n = 10$.

FIG. 7: Snapshots of the fluid profiles in $\delta t = 5$ intervals of the flow over increased number of perturbations of the substrate. Here $D = 1$, $w_x = 1$, and $w_y = 2$.

wavelengths. Figure 8 shows the flow down a vertical plane where a single perturbation is imposed close to the middle of a relatively wide computational domain, $L_y = 96$. Here, the perturbation is moved slightly off center so that we avoid imposing any symmetry. We see that so placed perturbation leads to an instability that propagates throughout the domain. In the process, fingers are formed, with those that develop closer to the imposed perturbation being longer, since these start growing earlier. The distance between the central fingers is

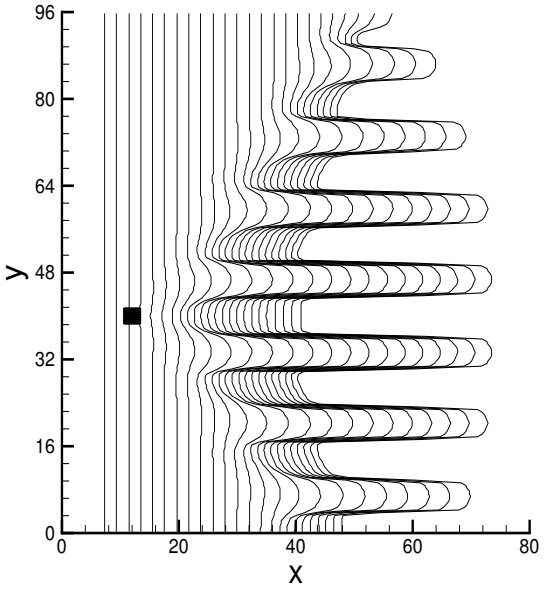

FIG. 8: Snapshots of the fluid profile in $\delta t = 2$ intervals of the flow down a vertical plane ($D = 0$) in the domain of width $L_y = 96$. A single perturbation ($w_x = w_y = 3$, $\delta = 0.5$) of the substrate is imposed at $x = 12$, $y = 40$.

almost exactly uniform, while toward the domain's edges (for small and large y's), this distance is modified by the boundaries' presence. The emerging wavelength (12.8 in Fig. 8) is rather close both to the one obtained computationally for a randomly perturbed contact line (e.g. Fig. 1), and to the one obtained by LSA.

The uniformness of the distance between fingers suggests that just a single perturbation may be sufficient to produce 'controlled' instability, i.e., that it is not necessary to control the flow by multiple perturbations as done experimentally[23] and computationally.[30] Of course, in physical experiments one also competes against the uncontrolled perturbations (noise) which may modify the flow. However, after an initial instability develops, we expect the system to be rather insensitive to additional noise-like perturbations. These expectations are supported by the computational and experimental results presented in Sec. VI.

Figure 9 shows the result for flow down an inclined plane, $D = 1$, with all other parameters as in Fig. 8. Note that the emerging patterns' shape is now triangular, as if the instability were induced by perturbing the contact line. Also, the distance between the tips is increased, leading to an average wavelength of approximately 16, very similarly to the case when the

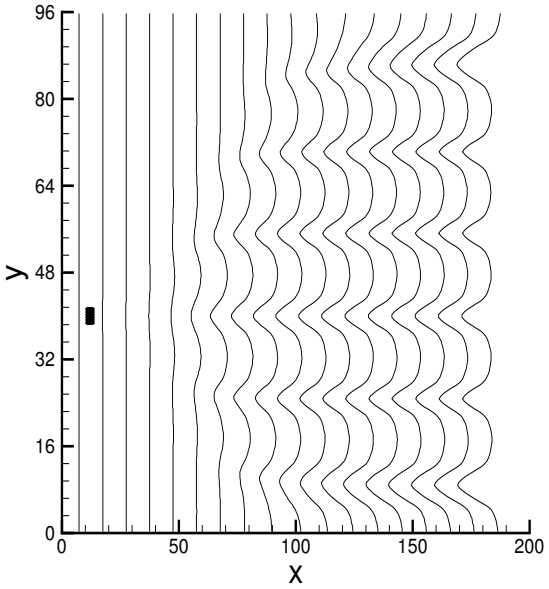

FIG. 9: Snapshots of the fluid profile in $\delta t = 10$ intervals of the flow down an inclined plane ($D = 1$). The other parameters are as in Fig. 8.

contact line is perturbed directly.[5,6] This increase of the average distance between patterns can be also seen in the experimental results shown in Fig. 2 (one needs to remember that the computational results are presented in nondimensional form, in contrast to the experimental figures). We conclude that, at least for the parameters we explore in this work, the main emerging patterns' features - their shape and distance - are independent of the nature of the perturbation that induces the instability.

We note in passing that the speed, u_t, of the instability propagation in the transverse, y, direction is not the same in Figs. 8 and 9. These figures imply that u_t is a decreasing function of the parameter D. In our nondimensional units, $u_t \approx 2$ for $D = 0$, and $u_t \approx 0.5$ for $D = 1$. We plan to analyze this spreading of instability in more detail elsewhere.

Continuous perturbations. Until now, we have explored the effect of isolated, point-like perturbations. Here we briefly discuss instabilities when a nontrivial continuous perturbation that crosses the domain in the transverse direction is present.

Figure 10 shows the results for a perturbed region of fixed width ($w_x = 3$), where the perturbation is a given sinusoidal shape in the y direction. Although w_x is constant, and it covers the whole domain's width, an instability is still produced, since different film's

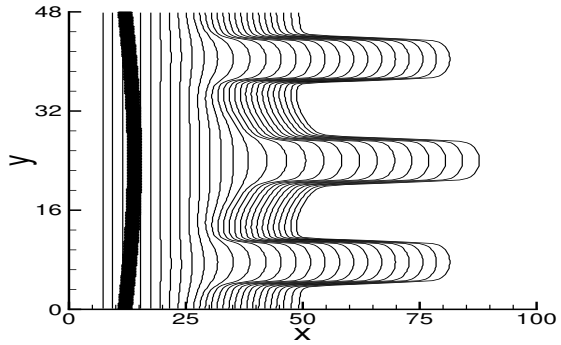

(a) *Period of the perturbation:* $p = 96$.

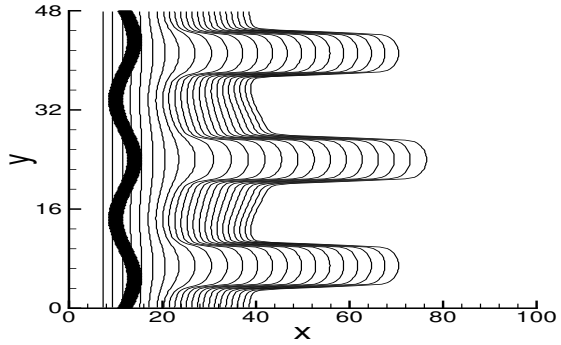

(b) *Period of the perturbation:* $p = 96/5$.

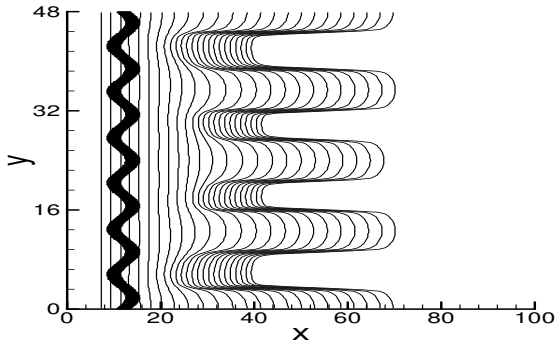

(c) *Period of the perturbation:* $p = 96/13$.

FIG. 10: Snapshots of the fluid profile in $\delta t = 2$ intervals of the flow down a vertical plane where we impose the continuous perturbations, of the width $w_x = 3$, and of various periods in the domain $L_y = 48$.

parts are perturbed at different times. Here, we see three examples of instability caused by these wave-like perturbations. We address first the patterns shown in Fig. 10b, where the imposed waves period is $p = 96/5 \approx 19$. Here, roots develop in the regions where the film reaches the perturbation first, while the tips form in between. Hence, the emerging pattern's wavelength equals the period of imposed perturbation. However, this may not hold in general. For example, in Fig. 10a, where $p = 96$, the roots location is determined by a rather involved interplay between the perturbation and the boundary conditions that require formation of a root or a tip at the boundaries. Since the fluid is first perturbed (slowed down) close to the boundaries ($y = 0, 48$), roots form there. Then, two fingers form at the distance from the roots that is determined by the capillary forces. Since the distance between these patterns is large enough to allow for secondary instability, an additional finger then forms in the domain's center.

Figure 10c shows a case where the perturbations' period, $p = 96/13 \approx 7.4$ is short enough to cause formation of patterns that only occasionally follow the rule that the surface perturbation's parts that are reached first and the emerging patterns roots should match. Again, the interplay between the imposed perturbation and boundary conditions leads to a final placement of fingers characterized by an average $\lambda = 12$.

Figure 11 shows a different kind of perturbation that can lead to instability. Here, a transverse perturbation is kept straight, but its width is modified. This width is varied between 2 and 4, and the period changes from $p = 6$ (a) to 12 (b), and 24 (c). First, we note that in the case $p < \lambda_c$, instability cannot develop, since the fluid cannot break the imposed symmetry (similar observation was made in the case of instability imposed by 'channels' of easy flow in our earlier work[30]). If $p > \lambda_c$, we generally observe tip formation in regions with narrow perturbation, and of roots where perturbation is wide. (viz. Fig. 11b). If p is as large as in Fig. 11c, a secondary instability develops (at $y = 12,\ 36$). This is similar to Fig. 5, where instability is induced by localized surface perturbations.

VI. INFLUENCE OF RANDOM SURFACE PERTURBATIONS (NOISE) ON INSTABILITY DEVELOPMENT IN SIMULATIONS AND EXPERIMENTS

In physical experiments one may expect the presence of random noise, due to either mechanical or chemical inhomogeneities. Furthermore, the contact line itself is typically

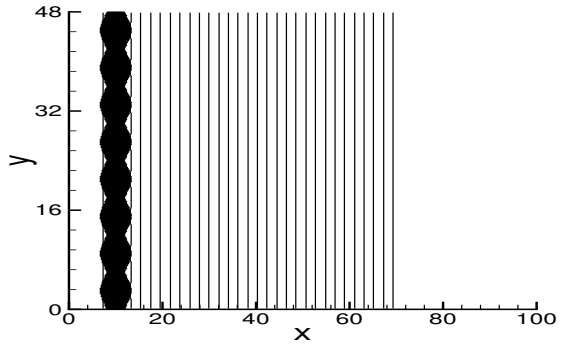

(a) *Period of the perturbation:* $p = 6$.

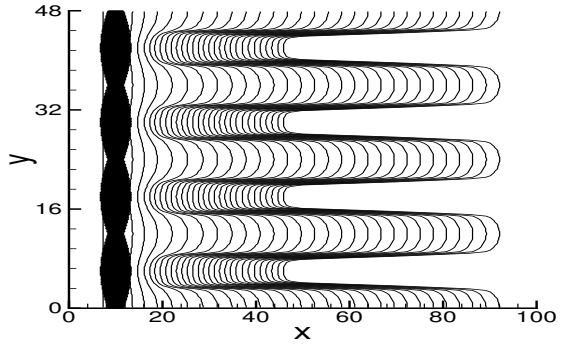

(b) *Period of the perturbation:* $p = 12$.

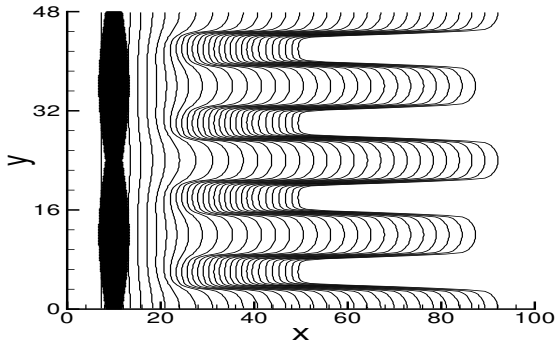

(c) *Period of the perturbation:* $p = 24$.

FIG. 11: Snapshots of the fluid profile in $\delta t = 2$ intervals of the flow down a vertical plane where we impose continuous perturbations of the width $w_x = 2 - 4$, and of various periods in the domain $L_y = 48$.

noisy. This kind of noise, that leads to instabilities as shown in Fig. 1, was analyzed in some detail in our previous works.[5,6] In particular, it is shown in Ref. 30 that the contact line noise may obstruct the formation of uniformly spaced patterns induced by regular surface's perturbations.

Here we analyze in more detail the influence of random *surface* perturbations on the flow stability and pattern formation. We note that these perturbations are characterized by their spatial extend that is much larger than the one that may be expected in the experiments on uniform, carefully prepared surfaces. While it is beyond the scope of this work to analyze computationally any realistic (microscopic) noise, we make a step in this direction by analyzing the influence of randomly distributed perturbations. Despite obvious differences, these simulations do provide significant insight into the main features of the experimental results.

In this section we concentrate on the following tasks:

- Show the influence of random surface perturbations on pattern formation in the simulations;
- Analyze an interplay between random and regular perturbations. In particular, show how 'better' control may be used to prevent surface perturbations from producing irregular patterns;
- Show experimental results that illustrate the fact that there exists a minimal distance between the imposed perturbations such that the fluid still follows the imposed surface features;
- Illustrate the effect of noise in experiments.

A. Development of instability caused by random surface perturbations

Figure 12 shows fluid profiles' snapshots for flow down a vertical plane, where the precursor thickness is modified by random perturbations. The parameters defining these perturbations are chosen randomly in a given range: the perturbations widths are $w_x = w_y = 3.0 \pm 1.0$, the x positions are $x_p = 12.0 \pm 1.0$, the depths are given by $\delta = 0.5 \pm 0.1$, and the distances between perturbations in the y direction are 7.0 ± 1.0. We choose relatively small average

distance between perturbations so that the system is not excited by the wavelengths close to λ^*. This relatively high frequency noise forces the system to decide on the emerging wavelengths on its own.

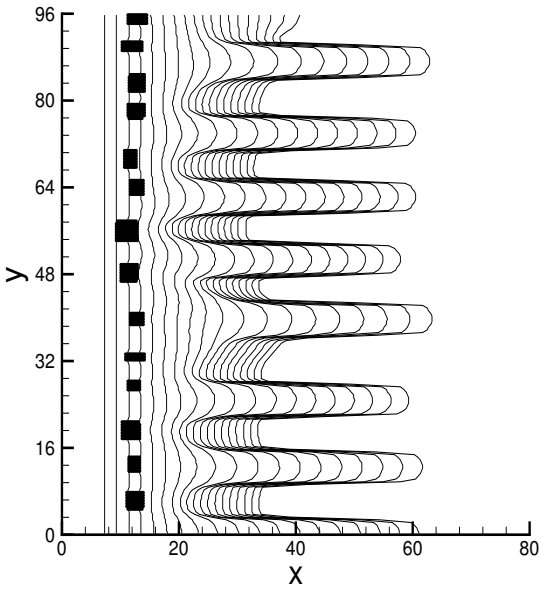

FIG. 12: Snapshots of the fluid profile in $\delta t = 2$ intervals of the flow down a vertical plane ($D = 0$), where precursor is perturbed by random perturbations as explained in the text.

The results shown in Fig. 12 are very similar to the ones shown in Fig. 1 that resulted from simulations where the contact line itself was perturbed. Additional simulations in which the seed for the random number generator has been modified, confirm that the patterns shapes, the average wavelengths, even the wavelengths' variances are very similar in these two kinds of simulations.

Figure 13 shows the results for the flow down an inclined plane, $D = 1$. The imposed perturbations are exactly the same as in Fig. 12 (note the larger x-range in this figure). The resulting patterns are again very close to those obtained in the simulations where the contact line has been perturbed.[5,6] Similarly to Figs. 6b - c, here we observe a delay in the instability development. For longer times, the profiles have almost reached steady state in an appropriate reference frame. This growth saturation has been found for all explored $D > 0$. Similar results have been recently observed in experiments where thermally driven flows are perturbed by laser pulses, leading to the formation of regular patterns.[43]

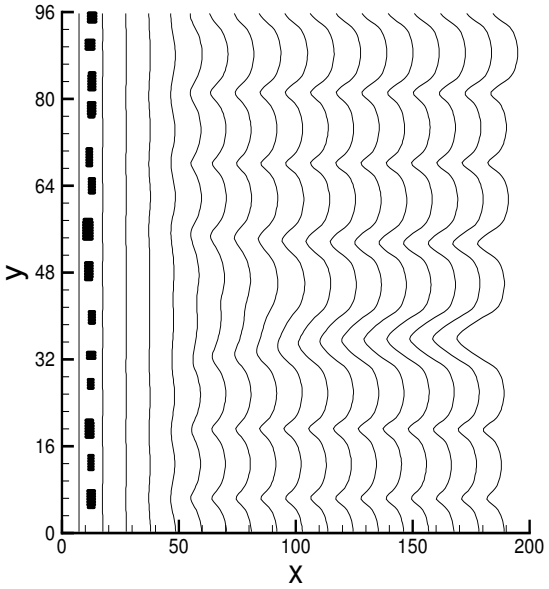

FIG. 13: Snapshots of the fluid profile in $\delta t = 10$ intervals of the flow down an inclined plane ($D = 1$), where the precursor is perturbed by random perturbations as explained in the text.

B. Interaction between noise and regular surface perturbations: Computational results

In our earlier work, we have shown that it is possible to control instability development by imposing infinite channels of 'easy' flow. That result is consistent with the experiments performed using thermally driven flows.[23] In these experiments, patterned surface (alternating stripes of bare and coated SiO_2) is prepared in a rather elaborate fashion, and the flow is driven by thermocapillary shear stress at the air-liquid interface. Correspondingly, the problem is more complicated (and characterized by much shorter length-scales) than the gravity driven flow outlined here. However, due to the similar nature of instability in these two problems, one expects that it should be possible to prepare a macroscopic experiment where the stripes (or any other desired pattern) are imposed on a homogeneous surface in some simple manner that allows for relatively straightforward experiments. Examples of such experiments are presented below in Sec. VI C.

We need to point out that in both thermally driven flows, and the experiments presented here, the fluid *wetting* properties are modified by the imposed perturbations. In our sim-

ulations, we perturb the *precursor film thickness*, essentially modifying the local resistance to the flow, but implicitly assuming complete wetting. Therefore, the manner in which the perturbations are imposed in our simulations is a simplified version of the physical problem.

The simplest way to understand the influence of noise is to add a 'weak' perturbation to otherwise well defined flow situation. Following this idea, Figure 14 shows the results that illustrate some of the effects that noise can have on the flow. The main goal of this figure is to analyze how the 'strength' of noise influences the pattern formation. (We note that the terms 'strength', as well as 'strong' and 'weak' below are used in the descriptive sense only. We do not attempt to analyze in detail the relative influence of the parameters characterizing a perturbation (its length, width, depth)). We also note that the flow can be very sensitive to the imposed noise's details. This point is made clear already by simple visual inspection of the different parts of Figure 14, in which most perturbations appear rather similar. However, the resulting fluid configurations can be very different.

All simulations presented on Fig. 14 are performed in domain of width $L_y = 24$, and have imposed two regular strong perturbations (we refer to them as the perturbations no. (2) and (3)) characterized by $w_y = 3$, (w_x is variable), $\delta = 0.5$ and centered at $y = 6, 18$, respectively. Without any additional perturbation, (2) and (3) lead to fingers' formation characterized by $\lambda = 12$, very similar to the ones shown in Fig. 14a. In addition to these two perturbations, there is an additional weak perturbation (no. (1)) imposed at $x = 10,\ y = 12$, that is typically more shallow ($\delta = 0.25$), and of decreased width.

Figure 14a shows the case where (1) is specified by $w_x = w_y = 2.0$, and (2, 3) by $w_x = 3.0$. The distance between the perturbations (more precisely, the distance in the streamwise direction between the center of (1) and the starting point of (2, 3)) is $x_d = 6$. Here, (1) is not strong enough to modify the flow significantly, so the long time flows development is almost the same as if (1) were not there. In Fig. 14b, we slightly increase the strength of (1) by choosing $w_x = w_y = 2.25$, and keeping everything else the same. This change is sufficient to completely modify the flow: in this case, (1) leads to the formation of a root downstream from its' position, in contrast to Fig. 14a. However, the configuration shown in Fig. 14b is energetically unfavorable, since the distance between the patterns is much larger than $2\lambda_c$ (see Fig. 5). Therefore, we expect formation of an additional finger which would reduce λ to 12. The initiation of this splitting process can be seen for the latest times shown in Fig. 14b.

Figure 14c illustrates that 'strengthening' of (2, 3) can balance a stronger perturbation

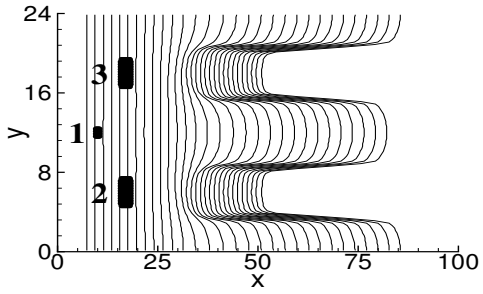

(a) *Weak first perturbation:* (1) ($x = 10$): $w_x = 2.0$, $\delta = 0.25$; (2, 3) ($x = 17$): $w_x = 3.0$, $\delta = 0.5$.

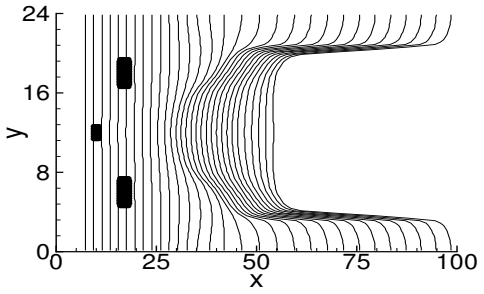

(b) *Strong first perturbation:* (1) ($x = 10$): $w_x = 2.25$, $\delta = 0.25$; (2, 3) ($x = 17$): $w_x = 3.0$, $\delta = 0.5$.

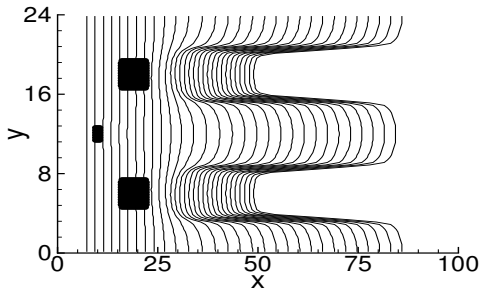

(c) *Long second perturbation:* (1) ($x = 10$): $w_x = 2.25$, $\delta = 0.25$; (2, 3) ($x = 19$): $w_x = 7.0$, $\delta = 0.5$.

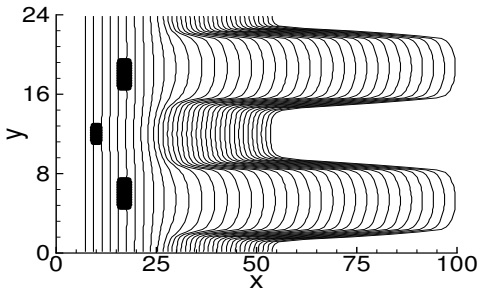

(d) *Deep first perturbation:* (1) ($x = 10$): $w_x = 2.0$, $\delta = 0.5$; (2, 3) ($x = 17$): $w_x = 3.0$, $\delta = 0.5$.

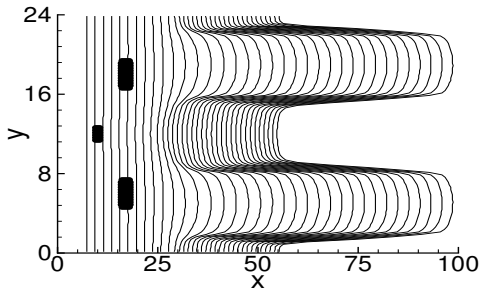

(e) *Large first perturbation:* (1) ($x = 10$): $w_x = 2.5$, $\delta = 0.25$; (2, 3) ($x = 17$): $w_x = 3.0$, $\delta = 0.5$.

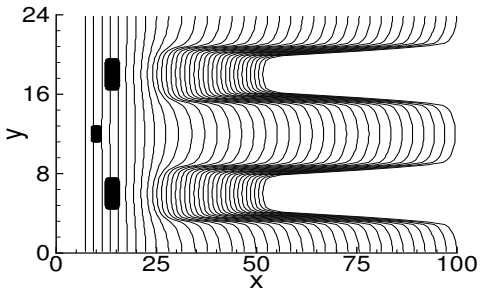

(f) *Short distance between perturbations:* (1) ($x = 10$): $w_x = 2.25$, $\delta = 0.25$; (2, 3) ($x = 12$): $w_x = 3.0$, $\delta = 0.5$.

FIG. 14: Snapshots of the fluid profile in $\delta t = 2$ intervals. Here the flow is perturbed by three perturbations. The first one (referred to as (1)) is always centered at $x = 10$ and its widths in the x and y directions are the same ($w_x = w_y$). The other two perturbations (referred to as (2) and (3)) are identical, have $w_y = 3.0$, $\delta = 0.5$, and are centered at $y = 6, 18$, and at variable x's.

(1). Here, (1) is the same as in Fig. 14b, but the length of (2, 3) is increased to $w_x = 7$, keeping x_d the same. As a result, we reach similar patterns as in the case where (1) was weaker. This is an example of a situation where longer perturbations (similar to the channels analyzed in Ref. 30) lead to formation of regular patterns that were not achieved by 'weaker' point-like perturbations.

Figure 14d returns to the point-like (2, 3) and explores the influence of the depth of (1). Here $\delta = 0.5$, while the widths are the same as in Figure 14a. This depth's increase has a dramatic influence, and completely modifies the emerging patterns. The result is almost identical as if (2, 3) were absent: two centrally positioned fingers form, the distance between them is $\lambda = 12$, and roots form at the boundaries ($y = 0, 24$). This configuration is favorable if strong (1) prevents formation of a finger tip in the domain's center at $y = 12$. The same result can be obtained if (1) is kept at the same depth, but its size is increased. This is illustrated in Fig. 14e, where the size of (1) is increased to $w_x = w_y = 2.5$, but its depth is $\delta = 0.25$. Figures 14d, e therefore illustrate how the spatial extend (w_x, w_y) and the depth, δ, combine to determine the total strength of a perturbation and its influence on the pattern formation process.

Figure 14f shows the case where the impact of (1) is weakened by reducing its range of influence. Here, (1, 2, 3) are identical to the ones used in Fig. 14b, but the centers of (2, 3) are shifted closer to (1), therefore affecting the flow earlier. Since (1) has less time/space to modify the flow, (2, 3) take over and lead to formation of different patterns compared to the case where the distance between perturbation is larger. Similar effect is also illustrated later in the experimental results shown in Sec. VI C.

Next, we proceed to more realistic examples of the influence of noise on pattern formation. Figures 15 - 17 combine random perturbations, similar to the ones used in Fig. 12, and regular perturbations at distances in the y directions that are decreased from $d = 12$ in Fig. 15 to $d = 10$ in Fig. 16, and to $d = 7$ in Fig. 17. The random perturbations are weaker than the regular ones and are positioned at (linearly stable) average distance of $d = 7$. These simulations are performed in the domain of width $L_y = 96$.

Figure 15 uses the distance, d, between regular perturbations that is close to the wavelength of maximum growth. Therefore, we expect that these perturbations will strongly influence the flow, leading to regularly spaced patterns characterized by the wavelength that coincides with d. This is really the case if the random perturbations are placed close to

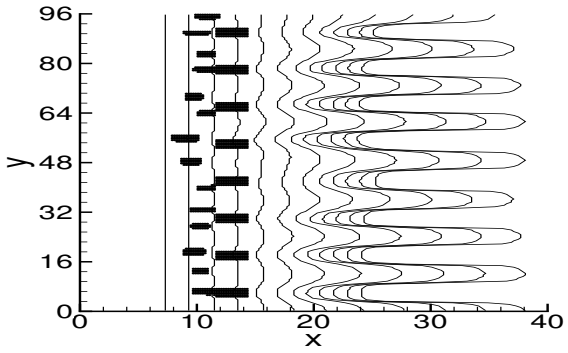

(a) *Short distance between perturbations:* $x_d = 3$.

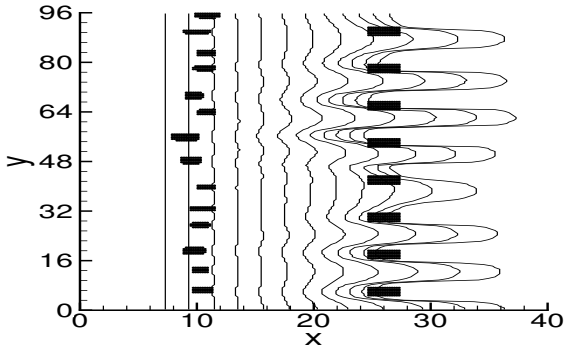

(b) *Long distance between perturbations:* $x_d = 16$.

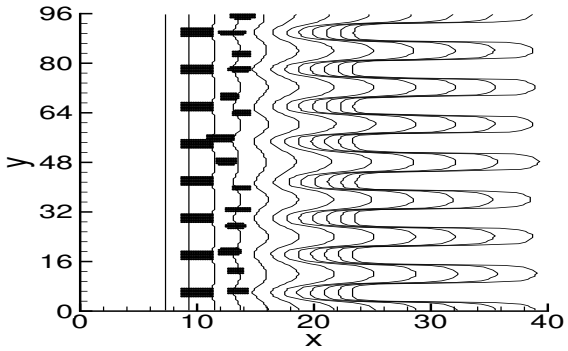

(c) *Random perturbations of perturbed flow:* $x_d = 3$.

FIG. 15: Snapshots of the fluid profile in $\delta t = 2$ intervals. The fluid is perturbed by a combination of regular perturbations ($w_x = w_y = 3.0$, $\delta = 0.5$, at the distance $d = 12$ apart in the y direction, positioned at $x = 26, 13, 10$ in (a,b,c), respectively), and random perturbations on average at $x = 10, 10, 13$, respectively. Other details are specified in the text.

the regular ones, as in Figure 15a. Here the average distance between the perturbations in the streamwise direction is $x_d = 3$. Therefore, the contact line does not have enough time to develop sufficiently long patterns prior to reaching the layer of regular perturbations. These regular perturbations then lead to patterns characterized by uniform distance and length. Perhaps surprisingly, these regular patterns are formed rather fast at a relatively short distance downstream from the zone of regular perturbations. If the distance x_d is increased, however, the fluid has more time do develop irregular patterns, and the regular perturbations' influence is not so strong. This effect is shown in Fig. 15b, where $x_d = 16$. Here, the patterns are less regular compared to Fig. 15a, although the regular perturbations' influence is still significant. The average wavelength (distance between patterns) is slightly larger than in Fig. 15a.

Figure 15c shows that the fluid that has already been perturbed by regularly spaced surface patterns is much less sensitive to random perturbations, compared to the unperturbed flow. We impose a regular perturbation pattern and then a group of random perturbations that are identical to the ones in Fig. 15a-b. The first regular array of perturbations produces uniformly spaced patterns which then reach the random perturbations. These random perturbations are placed close to the regular ones, so that the fluid does not have time/space to develop long fingers. However, even though the regular patterns are not yet fully formed, they are very stable with respect to this additional disturbance. These results show quite a remarkable stability of the already formed fluid patterns with respect to surface noise.

Figure 16 shows that it is not only the streamwise distance between random and regular perturbations that determines the eventual set of patterns. Here, although the regular perturbations follow the random ones very closely ($x_d = 3$, as in Fig. 15a) the influence of these regular perturbations is weakened by the fact that their distance in the y direction is only $d = 10$. Going back to LSA, we recall that the wavelength $\lambda = 10$ is only weakly unstable. Therefore, these perturbations cannot win against already formed patterns characterized by, on average, larger (and more unstable) wavelengths. The average distance between patterns is the same as in Fig. 15b, despite the fact that the regular perturbations are spaced closer to each other.

Figure 17 shows the resulting patterns where the distance between regular perturbations is $d = 7$. Since $d = 7$ is less than λ_c, the fluid does not follow the imposed regular perturbations at all, and instead develops randomly distributed patterns. The average distance between

the patterns is close to the wavelength of maximum growth, and in this case is the same as in Figs. 15b and 16. In what follows, we present the connection of these results to physical experiments.

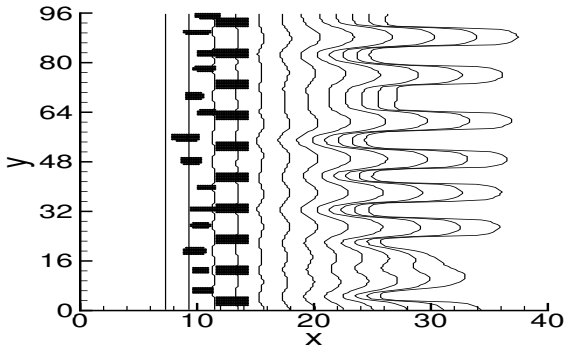

FIG. 16: Snapshots of the fluid profile in $\delta t = 2$ intervals. The fluid is perturbed by a combination of regular perturbations ($w_x = w_y = 3.0$, $\delta = 0.5$, at the distance $d = 10$ apart in the y direction, positioned at $x = 13$), and of random perturbations identical to the ones in Fig. 15a-b.

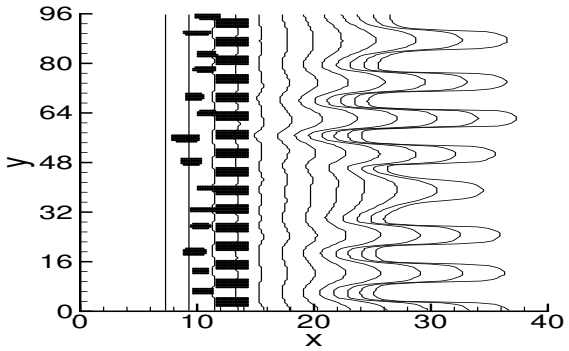

FIG. 17: Snapshots of the fluid profile in $\delta t = 2$ intervals. The fluid is perturbed by a combination of regular perturbations ($w_x = w_y = 3.0$, $\delta = 0.5$, at the distance $d = 7$ apart in the y direction, positioned at $x = 13$), and of random perturbations identical to the ones in Fig. 15a-b.

C. Interaction between noise and regular surface perturbations: experimental results

Figures 18 - 20 show the experimental patterns that result as PDMS flows over surface that is modified by the presence of stripes. These stripes are prepared by covering some glass plate's portions by an oil-based paint. The apparent contact angle of the PDMS on the stripes is significantly larger than on the glass not covered by the paint. Therefore, PDMS tries to avoid flowing on the painted stripes and flows in the 'easy' flow regions instead. The experimental setup is otherwise identical to the one used to obtain the data shown in Fig. 2, with the inclination angle of $\alpha = 5$ degrees. Due to this small inclination, the 'natural' contact line instability (that would develop on a macroscopically homogeneous surface without any imposed surface perturbations) grows rather slowly (see also Fig. 2c), so that the contact line is very weakly corrugated by the time the fluid reaches the striped region. By repeating the experiment with identical, but water-based paint stripes, we verified that it is actually the variation of wetting properties which is the source of instability, and not the mechanical perturbation imposed by applying a very thin layer of paint. In the latter case of water-based paint, the fluid flow is unperturbed by the stripes' presence. Note that the fluid actually flows over the stripes (this may not be obvious from the figures), eventually completely covering the whole domain. We think of the experiments shown in Figs. 18 - 20 as an experimental analog of the simulations shown in Figs. 15 - 17. The stripes in experiments play the role of strong, regular perturbations in simulations, while irregular perturbations are naturally provided in experiments by microscopic surface inhomogenities.

Figure 18 shows that the stripes' presence (width of 2.5 cm, and the distance between neighbors of 2.5 cm) is sufficient to induce instability and formation of long fingers in between the stripes (similarly to the simulations shown in Fig. 15a). This particular configuration is chosen since the imposed wavelength is close to the natural wavelength that develops in the case of the flow on plane glass, see Fig. 2c. It is also close to the estimate that goes back to Huppert[2], who predicts that the emerging wavelength is given by $\lambda_e \approx 7.5\sqrt{A}\sigma/(\rho g \sin\alpha)$, where A is the cross sectional fluid area. With our flow and fluid parameters, this estimate gives $\lambda_e \approx 4.2$ cm. One can show that a similar estimate also results from LSA.

Figure 19 shows that if the distance between stripes is decreased, and everything else left the same, very different patterns are obtained. Here, the stripes are 0.65 cm wide,

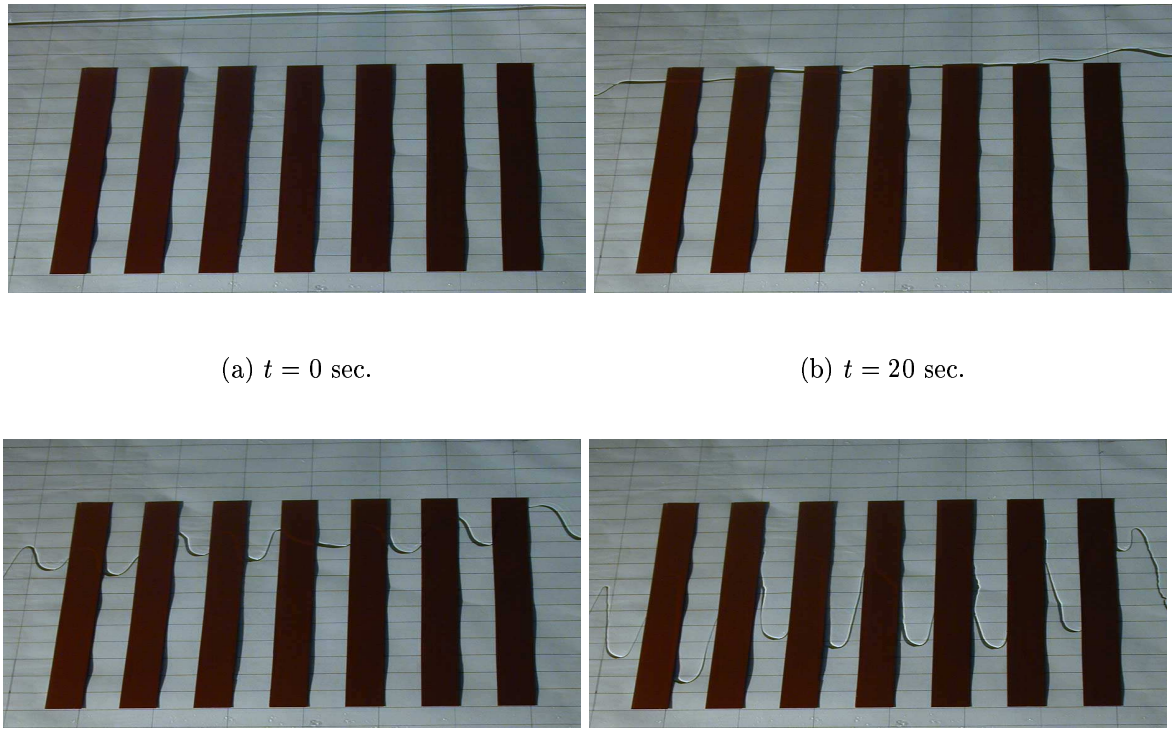

(a) $t = 0$ sec. (b) $t = 20$ sec.

(c) $t = 60$ sec. (d) $t = 180$ sec.

FIG. 18: Snapshots of the PDMS front on 5 degrees incline as it flows over 2.5 cm wide stripes (oil paint), with spacing of 2.5 cm in between. The fluid is released at time $t = 0$, 8 cm above the stripes' start. The amount of fluid is 25 grams. Note that the fluid actually flows on the stripes but it is slowed down significantly.

and the distance between them is also 0.65 cm. In this case, the fluid follows the imposed perturbations only partially, similarly to the computational results shown in Fig. 17. Clearly, the average wavelength is much larger than the imposed patterns' periodicity.

Next we proceed to discuss the influence of noise on the flow. In Fig. 15 we discussed this issue computationally (see also Ref. 30). Figure 15 shows that if the contact line is perturbed by random noise, and then let to flow over striped region, the outcome depends on the distance between the release point and the beginning of striped region. Figure 20 illustrates this effect in the experiments. Here, the fluid's release point is 4 cm further away from the striped region's beginning, compared to Fig. 18. Clearly, the patterns that form are now much more irregular. Since the instability has more time to develop prior to reaching the striped region, the stripes' influence is not sufficient to reorganize the flow. By

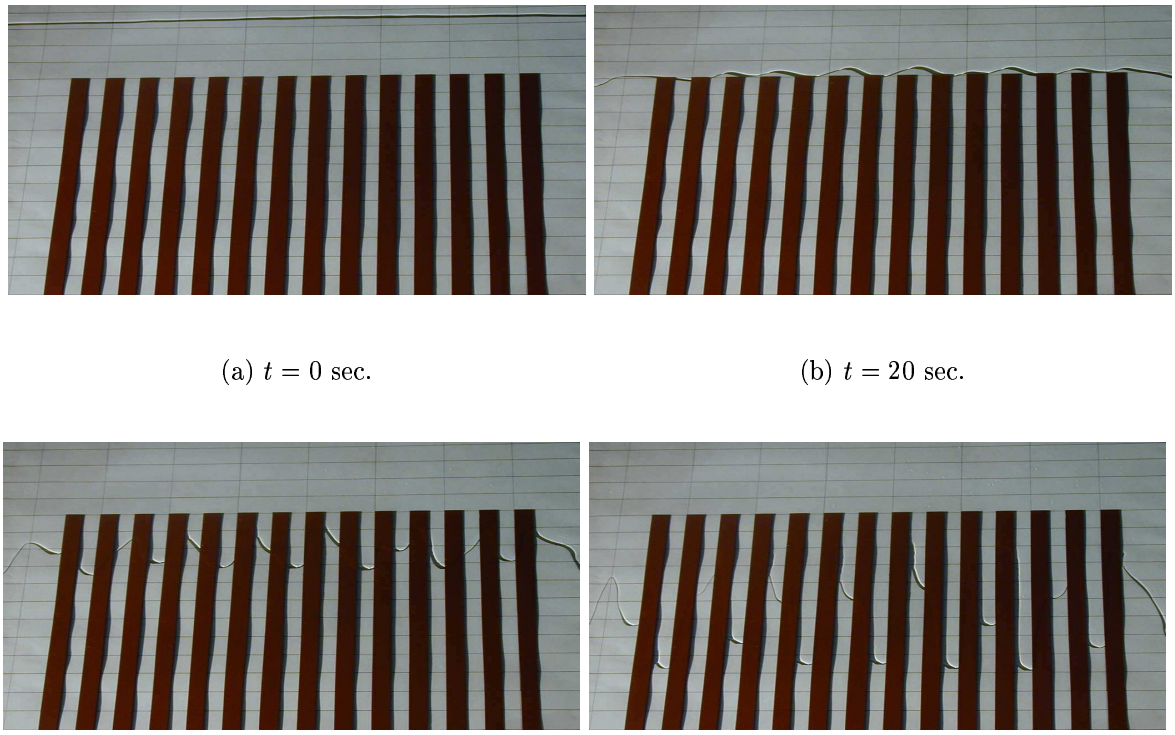

(a) $t = 0$ sec. (b) $t = 20$ sec.

(c) $t = 60$ sec. (d) $t = 180$ sec.

FIG. 19: Snapshots of the PDMS front as it flows over 0.65 cm wide stripes (oil paint), with spacing of 0.65 cm in between. The setup is the same as in Fig. 18, except for the configuration of stripes.

performing additional experiments (not shown here for brevity) with different fluid volumes, we have verified that the difference between Figs. 18 and 20 does not result from the fluid thickness' change at the moment of arriving at the striped region.

Additional experiments have shown that, in some cases, longer stripes could stabilize the flow better than shorter ones, similarly as illustrated in Fig. 14. This applies in particular when the imposed distance between the evolving patterns is close to the critical wavelength. We have also analyzed the influence of changing fluid volume. Decreased volume leads to thinner films and shorter length scales, as expected based on simple scaling arguments. This allows, for example, the fluid to follow the stripes as imposed in Fig. 19. We note that this observation is also consistent with the analysis[28] of the dewetting process on heterogeneous substrates.

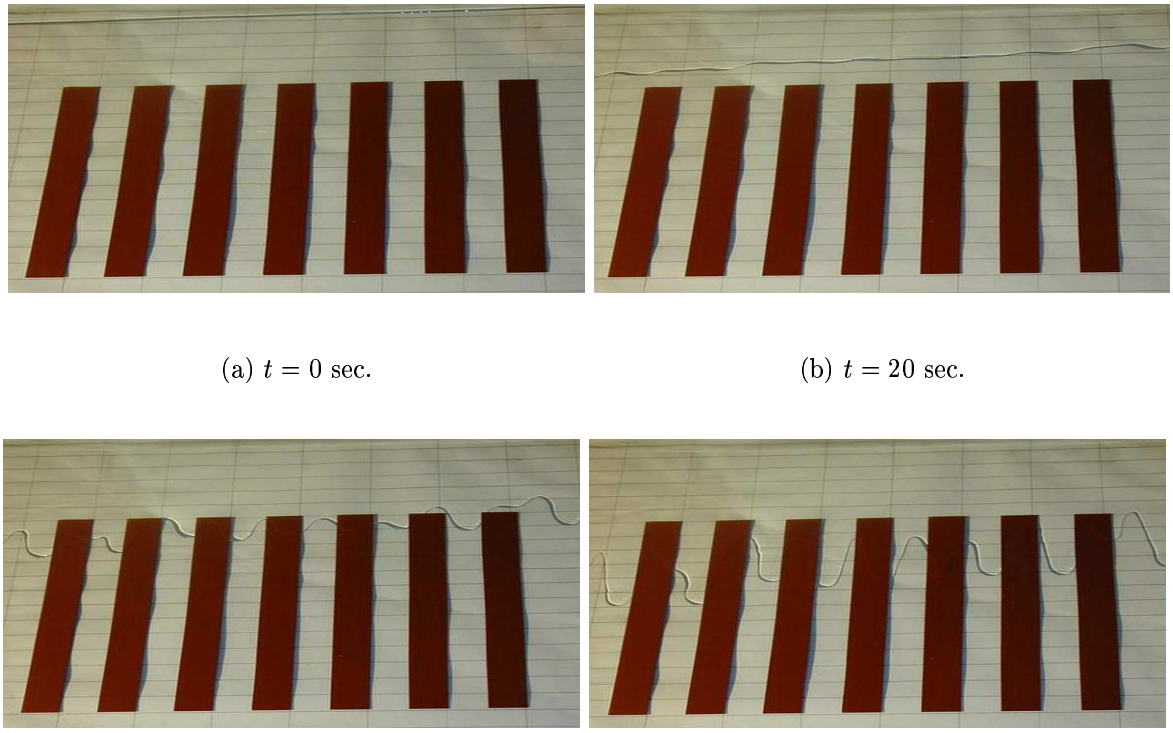

(a) $t = 0$ sec. (b) $t = 20$ sec.

(c) $t = 60$ sec. (d) $t = 180$ sec.

FIG. 20: Snapshots of the PDMS front as it flows over 2.5 cm wide stripes (oil paint), with spacing of 2.5 cm in between. The fluid is released at time $t = 0$, 12 cm above the stripes' start. The configuration is identical to the one shown in Fig. 18, except for the release point.

VII. CONCLUSION

By combination of computational and experimental techniques, we outline the connection between natural instability of gravity driven thin fluid films on homogeneous surfaces, and the flow of thin films on patterned (striped) surfaces. Heterogeneity of the surface is modeled by varying the precursor film's thickness, therefore modifying the local resistance to fluid motion. One observation is that the patterns' characteristics that form in the system where the surface properties (precursor film) are modified, are very similar to the ones resulting from contact line perturbations. Next, one finds that by imposing local, point-like perturbations, similar results can be produced as in the case of long channel-like perturbations. In addition, we also analyze continuous transverse perturbation and show that these can be also used to produce regularly spaced patterns.

One issue which we analyze in detail is the influence of noise on the pattern formation, where noise is imposed by randomly positioned point-like perturbations. Unperturbed fluid fronts are found to be very sensitive to this type of perturbations, although significant time can be needed for the front corrugations to start developing, in particular for small inclination angles. However, if patterns are already formed, they are almost insensitive to the random perturbations of the surface. This conclusion has been reached both in simulations and in experiments.

Our theoretical and computational methods are currently being developed to include modeling of the details of (possibly heterogeneous) surface chemistry. However, already the present model shows a lot of potential, since it has successfully reproduced the qualitative features of experimentally observed pattern formation in the experiments reported here, as well as of the experiments involving thermally driven thin films. Our future work will proceed in the direction of developing better understanding of the relevant issues that determine the dynamics of microflows, including their control and applications.

Acknowledgments. L. K. acknowledges help with experiments by an undergraduate student of NJIT, Rafal Turek, and thanks Gregory Kriegsman for help with student summer support. The authors acknowledge support by NSF grant No. INT-0122911.

* E-mail:kondic@oak.njit.edu

† E-mail:jdiez@exa.unicen.edu.ar

[1] N. Silvi and E. B. Dussan V. On the rewetting of an inclined solid surface by a liquid. *Phys. Fluids*, 28:5, 1985.

[2] H. Huppert. Flow and instability of a viscous current down a slope. *Nature*, 300:427, 1982.

[3] M. F. G. Johnson. *Experimental study of rivulet formation on an inclined plate by fluorescent imaging.* PhD thesis, Northwestern University, 1997.

[4] M. F. G. Johnson, R. A. Schluter, M. J. Miksis, and S. G. Bankoff. Experimental study of rivulet formation on an inclined plane by fluorescent imaging. *J. Fluid. Mech.*, 394:339, 1999.

[5] J. Diez and L. Kondic. Contact line instabilites of thin liquid films. *Phys. Rev. Lett.*, 86:632, 2001.

[6] L. Kondic and J. Diez. Contact line instabilities of thin film flows: Constant flux configuration. *Phys. Fluids*, 13:3168, 2001.

[7] S. M. Troian, E. Herbolzheimer, S. A. Safran, and J. F. Joanny. Fingering instabilities of driven spreading films. *Europhys. Lett.*, 10:25, 1989.

[8] M. A. Spaid and G. M. Homsy. Stability of Newtonian and viscoelastic dynamic contact lines. *Phys. Fluids*, 8:460, 1996.

[9] A. L. Bertozzi and M. P. Brenner. Linear stability and transient growth in driven contact lines. *Phys. Fluids*, 9:530, 1997.

[10] Y. Ye and H. Chang. A spectral theory for fingering on a prewetted plane. *Phys. Fluids*, 11:2494, 1999.

[11] R. O. Grigoriev. Contact line instability and pattern selection in thermally driven liquid films. *Phys. FLuids*, 15:1363, 2003.

[12] J. M. Davis and S. M. Troian. On a generalized approach to the linear stability of spatially nonuniform thin film flows. *Phys. Fluids*, 15:1344, 2003.

[13] S. Kalliadasis, C. Bielarz, and G. M. Homsy. Steady free-surface thin film flows over topography. *Phys. FLuids*, 12:1889, 2000.

[14] C. Bielarz and S. Kalliadasis. Time-dependent free-surface thin film flows over topography. *Phys. FLuids*, 15:2512, 2003.

[15] L. E. Stillwagon and R. G. Larson. Leveling of thin films over uneven substrates during spin coating. *Phys. Fluids A*, 2:1937, 1990.

[16] K. Hoffmann, B. Wagner, and A. Münch. On the generation and spreading of 'finger' instabilities in film coating processes. In H. J. Bungartz, F. Dust, and C. Zenger, editors, *Lecture Notes in Computational Science and Engineering, vol. 3*. Springer-Verlag, 1999.

[17] C. Y. Wang. Flow over surfaces with parallel grooves. *Phys. Fluids*, 15:1114, 2003.

[18] L. M. Hocking. A moving fluid interface on a rough surface. *J. Fluid. Mech.*, 76:801, 1976.

[19] M. J. Miksis and S. H. Davis. Slip flow over rough and coated surfaces. *J. Fluid. Mech.*, 273:125, 1994.

[20] J. Drelich, J. L. Wilbur, J. D. Miller, and G. M. Whitesides. Contact angles for liquid drops at a model heterogenous surface consisting of alternating and parallel hydrophobic/hydrophylic strips. *Langmuir*, 12:1913, 1996.

[21] L. W. Schwartz. Hysteretic effects in droplet motions on heterogenous substrates: Direct numerical simulations. *Langmuir*, 14:3440, 1998.

[22] L. W. Schwartz and R. R. Eley. Simulation of droplet motion of low-energy and heterogenous surfaces. *J. Colloid Interface Sci.*, 202:173, 1998.

[23] D. E. Kataoka and S. M. Troian. Patterning liquid flow on the microscopic scale. *Nature*, 402:794, 1999.

[24] A. A. Darhuber, S. M. Troian, S. M. Miller, and S. Wagner. Morphology of liquid microstructures on chemically patterned surfaces. *J. Appl. Phys.*, 87:7768, 2000.

[25] A. A. Darhuber, S. M. Troian, J. M. Davis, S. M. Miller, and S. Wagner. Selective dip-coating of chemically micropatterned surfaces. *J. Appl. Phys.*, 88:5119, 2000.

[26] A. A. Darhuber, S. M. Troian, and W. W. Reisner. Dynamics of capillary spreading along hydrophylic microstripes. *Phys. Rev. E*, 64:031603, 2001.

[27] N. Garnier, R. O. Grigoriev, and M. F. Schatz. Optical manipulation of microscale fluid flow. *Phys. Rev. Lett.*, 91:054501, 2003.

[28] L. Brusch, H. Kühne, U. Thiele, and M. Bär. Dewetting of thin films on heterogenous substrates: Pinning versus coarsening. *Phys. Rev. E*, 66:011602, 2002.

[29] K. Kargupta and A. Sharma. Templating of thin films induced by dewetting on patterned surfaces. *Phys. Rev. Lett.*, 86:4536, 2001.

[30] L. Kondic and J. Diez. Flow of thin films on patterned surfaces: Controlling the instability.

Phys. Rev. E, 65:045301, 2002.

[31] L. Kondic and A. L. Bertozzi. Nonlinear dynamics and transient growth of driven contact lines. *Phys. Fluids*, 11:3560, 1999.

[32] A. L. Bertozzi, G. Grün, and T. P. Witelski. Dewetting films: bifurcations and concentrations. *Nonlinearity*, 14:1569, 2001.

[33] K. B. Glasner and T. P. Witelski. Coarsening dynamics of dewetting films. *Phys. Rev. E*, 67:016302, 2003.

[34] L. M. Pismen and Y. Pomeau. Disjoining potential and spreading of thin liquid layers in the diffuse-interface model coupled to hydrodynamics. *Phys. Rev. E*, 62:2480, 2000.

[35] U. Thiele, M. G. Velarde, K. Neuffer, and Y. Pomeau. Film rupture in the diffuse interface model coupled to hydrodynamics. *Phys. Rev. E*, 64:031602, 2001.

[36] J. Diez and L. Kondic. Computing three-dimensional thin film flows including contact lines. *J. Comp. Phys.*, 183:274, 2002.

[37] H. P. Greenspan. On the motion of a small viscous droplet that wets a surface. *J. Fluid Mech.*, 84:125, 1978.

[38] E. B. Dussan V. The moving contact line: the slip boundary condition. *J. Fluid Mech.*, 77:665, 1976.

[39] L. M. Hocking and A. D. Rivers. The spreading of a drop by capillary action. *J. Fluid. Mech.*, 121:425, 1982.

[40] J. Diez, L. Kondic, and A. L. Bertozzi. Global models for moving contact lines. *Phys. Rev. E*, 63:011208, 2001.

[41] L. Kondic. Instabilities in the flow of thin liquid films. *SIAM Review*, 45:95, 2003.

[42] P. G. de Gennes. Wetting: Statics and dynamics. *Rev. Mod. Phys.*, 57:827, 1985.

[43] T. Witelski and J. Sur, 2003. private communication.

[44] In a forthcoming paper we probe micrometric films obtained by releasing fixed volumes of PDMS on a vertical glass, and quantitatively compare the thickness profiles and contact line dynamics with numerical simulations.